

Article

New Evidence of the Brizziite, Sodium Antimonate from the Central Paratethys Sea Strata in Poland

Bożena Gołębiowska ^{*}, Monika Pilarz and Krzysztof Bukowski 

Faculty of Geology, Geophysics and Environmental Protection, AGH University of Science and Technology, Mickiewicza 30, 30-059 Kraków, Poland; pilarz@agh.edu.pl (M.P.); buk@agh.edu.pl (K.B.)

* Correspondence: goleb@agh.edu.pl

Abstract: Brizziite, a rare sodium antimonate ($\text{NaSb}^{5+}\text{O}_3$), and fluorcalciroméite ($(\text{Ca,Na})_2\text{Sb}^{5+}_2\text{O}_6\text{F}$), have been identified in two boreholes (Pasternik and Włosienica) which are situated 50 km apart. Both wells are located west of Krakow, Poland, and were drilled in the Miocene strata of the Paratethys Sea (a remnant of the Tethys Ocean). The Sb minerals are scattered in a solidified light blue silica gel within marls and layered clays. They occur most often as anhedral grains up to 20 μm in size. The presence of these phases was confirmed by Raman spectroscopy (RS) and X-ray diffraction (XRD). The brizziite from this study represents a secondary mineral after the alteration of roméite within a supergene zone, or crystallization from Sb-rich solutions derived by the leaching of the weathered primary roméite. Hence, the calcium and fluorine admixtures in their composition, determined by EPMA, indicate intergrowths of brizziite and roméite on the micro- to crypto-scale. The presence of the antimony in the study area is related to rejuvenated Old-Paleozoic polymetallic ore-mineralization occurring in the basement of the Krakow-Silesia Monocline. The phenomenon of the repeatability of brizziite in Pasternik and Włosienica, distant by several tens of kilometers, can be explained by the following three steps: (i) the penetration of the chloride ions from the drying up seawaters of the Paratethys Sea into the Miocene groundwater system, (ii) the mobilization of Sb^{5+} in the form of chloride complexes, and, finally, (iii) the transportation of the Sb-bearing solutions within the marly and clay sediments.

Keywords: brizziite; fluorcalciroméite; Sb mineralization; Polish Carpathian Foredeep; the Paratethys Sea; Miocene



Citation: Gołębiowska, B.; Pilarz, M.; Bukowski, K. New Evidence of the Brizziite, Sodium Antimonate from the Central Paratethys Sea Strata in Poland. *Minerals* **2021**, *11*, 1403. <https://doi.org/10.3390/min11121403>

Academic Editors:
Hans-Jürgen Gawlick,
Michał Krobicki and Laszlo Bujtor

Received: 12 November 2021
Accepted: 7 December 2021
Published: 11 December 2021

Publisher's Note: MDPI stays neutral with regard to jurisdictional claims in published maps and institutional affiliations.



Copyright: © 2021 by the authors. Licensee MDPI, Basel, Switzerland. This article is an open access article distributed under the terms and conditions of the Creative Commons Attribution (CC BY) license (<https://creativecommons.org/licenses/by/4.0/>).

1. Introduction

Brizziite ($\text{NaSb}^{5+}\text{O}_3$) is a rare sodium antimonate, found only in two localities so far, as follows: the Cetine mine and the Pereta mine, both in Tuscany, Italy [1,2]. It co-occurs there with other sodium antimonates. At the first location, it represents a secondary product of stibnite in a weakly silicified limestone [1]. It has also been observed in waste material and slag derived from mining operations [3]. The encrustations of brizziite are microscopic aggregates of platy crystals and, occasionally, thin tabular crystals. The origin of this epigenetic mineralization is related to a late phase of the Pliocene–Pleistocene Apennine magmatism [4]. Brizziite from Pereta, in flat elongated aggregates, co-occurs with mopungite ($\text{NaSb}^{5+}(\text{OH})_6$) and ottensite ($\text{Na}_3(\text{Sb}_2\text{O}_3)_3(\text{SbS}_3)\cdot 3\text{H}_2\text{O}$), which spread on stibnite. The largest brizziite crystals reach a length of 50 μm . Brizziite from the Pereta mine is also a secondary phase after the Sb primary minerals.

The roméite-group minerals belong to the pyrochlore supergroup, whose general formula can be written down as $\text{A}_{2-m}\text{B}_{2 \times 6-w}\text{Y}_{1-n}$, including the following [5,6]:

A = Na, Ca, Ag, Mn, Sr, Ba, Fe²⁺, Pb, Sn²⁺, Sb³⁺, Bi³⁺, Y, REE, Sc, U, Th, □ (=vacancy) and H₂O; B = Ta, Nb, Ti, Sb⁵⁺, W, V⁵⁺, Sn⁴⁺, Zr, Hf, Fe³⁺, Mg, Al and Si; X = O²⁻, (OH)⁻ and F; Y = (OH)⁻, F⁻, O²⁻, □, H₂O, K⁺, Cs⁺, Rb⁺. The Sb⁵⁺ is the main cation at the B-site within the roméite-group minerals [5,6].

The Y-site chemistry of roméite varies from one locality to another; it can be dominated by F, OH, or be fully vacant [5]. In the roméite structure, we can observe many substitutions between the A- and B- and the A- and Y-sites. According to Brugger et al. [6], the A-site vacancies in roméite are controlled by the primary crystallization conditions, not by post-crystallization alteration. The Commission on New Minerals, Nomenclature and Classification (CNMNC) accepts four minerals of the roméite group, as follows: oxycalcioroméite (Ca₂Sb⁵⁺₂O₇), oxyplumboroméite (Pb₂Sb₂O₇), fluorcalcioroméite [(Ca,Na)Sb⁵⁺₂O₆F], and hydroxycalcioroméite [(Ca,Sb³⁺)₂(Sb⁵⁺,Ti⁴⁺)₂O₆OH]. This complicated structural group has been described by many authors [5–11]. Roméite has been observed in metamorphic rocks and hydrothermal veins and is associated with antimony mineralization.

Antimony belongs to the group of critical elements. China, Bolivia, and Russia are countries with the main resources of the element. Antimony is used to produce flame retardant materials in plastics, coatings, and electronics. It is also used as a decolorizing ingredient in glass, in producing batteries, PET polymers, and alloys [12,13]. The industrial use of antimony is mainly associated with stibnite. However, attention is paid to finding other sources of antimony, e.g., by recycling end-of-life products or by recovering antimony from industrial process residues. Antimony residues are obtained by processing Au, Cu, and Pb ores with high contents of antimony [12]. The mineralization presented in this paper becomes very interesting due to the potential wide mineralization area.

The authors present the results of the mineralogical investigations of brizziite and coexisting roméite, suggest the genesis of rare brizziite other than the hypotheses on its origin put forward previously, and discuss why such a rare mineral occurs in boreholes distant over several tens of kilometers from each other.

2. Geological Setting

The study area is located near Krakow, in the Polish part of the Carpathian Foredeep, and was formed in the Miocene as a peripheral foreland basin [14]. It constituted the northernmost part of the epicontinental Central Paratethys Sea (Figure 1A), which separated from the remnants of the northern Tethys Ocean in the Oligocene (~34 Ma) [15,16]. The Central Paratethys, a chain of interconnected epicontinental basins in which water was freely exchanged, existed in various configurations from the early Oligocene to the Late Miocene [17]. Episodically, marine hydrological connections between the different basins were reduced due to complex tectonic and/or glacio-eustatic processes [18]. During the Middle Miocene (Langhian), tectonic movements, associated with the folding and uplift of the Carpathians, led to marine transgression into the adjacent areas. Marine deposits of sandstones, mudstones, and clays with thicknesses ranging from tens to hundreds of meters were formed. At the same time, intense volcanism took place in the Carpathian area, which left behind levels of tuffs and tuffites [19–22]. Miocene profiles of the Langhian (early Badenian) sediments have been undisturbed, and only in a narrow zone extending along the Carpathian overthrust are they folded. The mineralization described in this paper is derived from this sub-evaporite series (Figure 2), the age of which has been determined as Langhian (Early Badenian) based on microfaunal studies [23]. The drilling profiles described in this paper are located to the west of Krakow (Figure 1C), where the width of the Carpathian Foredeep is only a few kilometers (5–10 km). The basement rocks of the Miocene sediments occur there at relatively shallow depths. That elevation of the Paleozoic and Mesozoic terrain (“Krakow Bolt”) has partially restricted the free exchange of water between the two parts of the basin [24]. A sequence of grabens and dislocation zones have been observed within the consolidated basement [25]. Also nearby is the 500 m wide Krakow–Lubliniec Fault Zone (KLFZ), which cuts and dislocates all of the Precambrian and Paleozoic rock series (Figure 1C). Much of this dislocation resurfaced in the Neogene

time, during the remodeling of the region. Parallel faults formed, creating newly separated grabens (e.g., the Krzeszowice Graben).

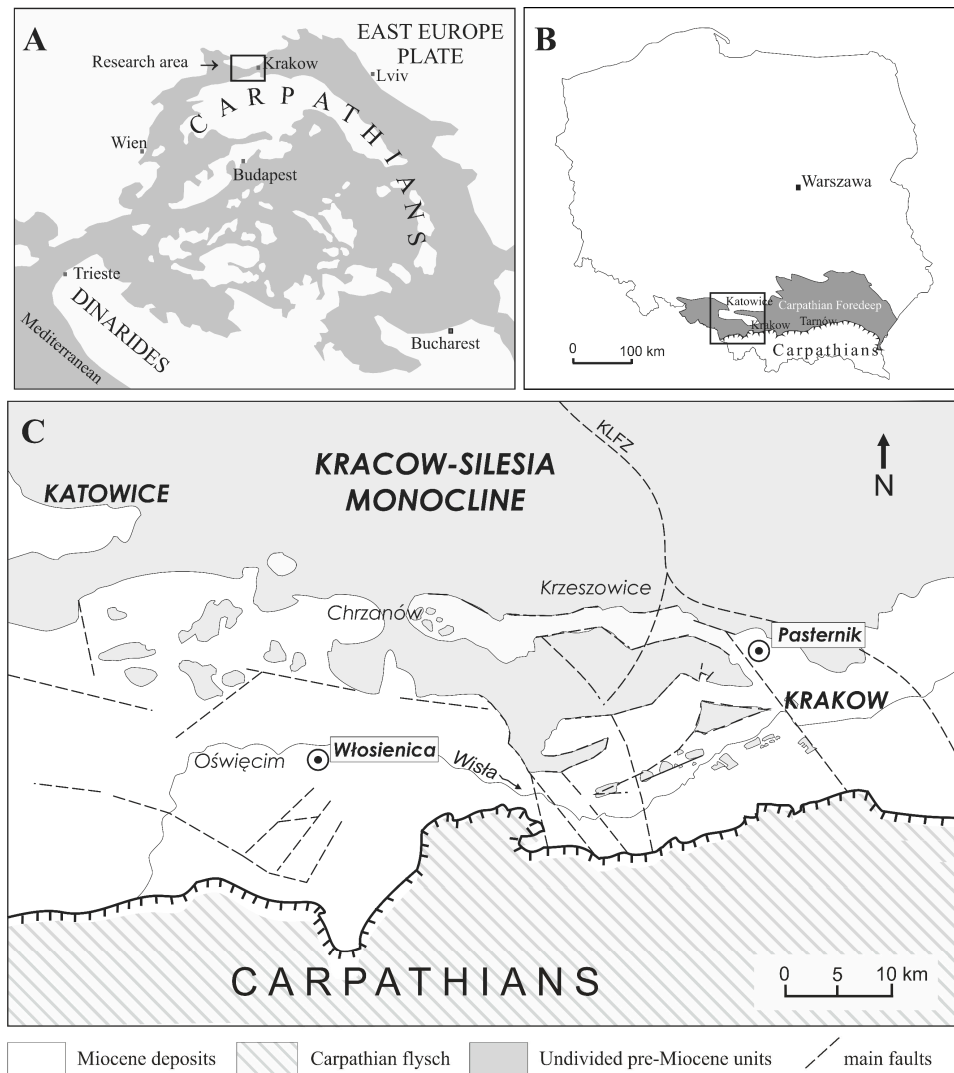


Figure 1. Location map of the study area: (A)-location within the Central Paratethys (after [26]); (B)-Schematic map of Poland with Carpathian Foredeep (after [24]); (C)-Simplified geological map of the study area with location of boreholes (after [23]).

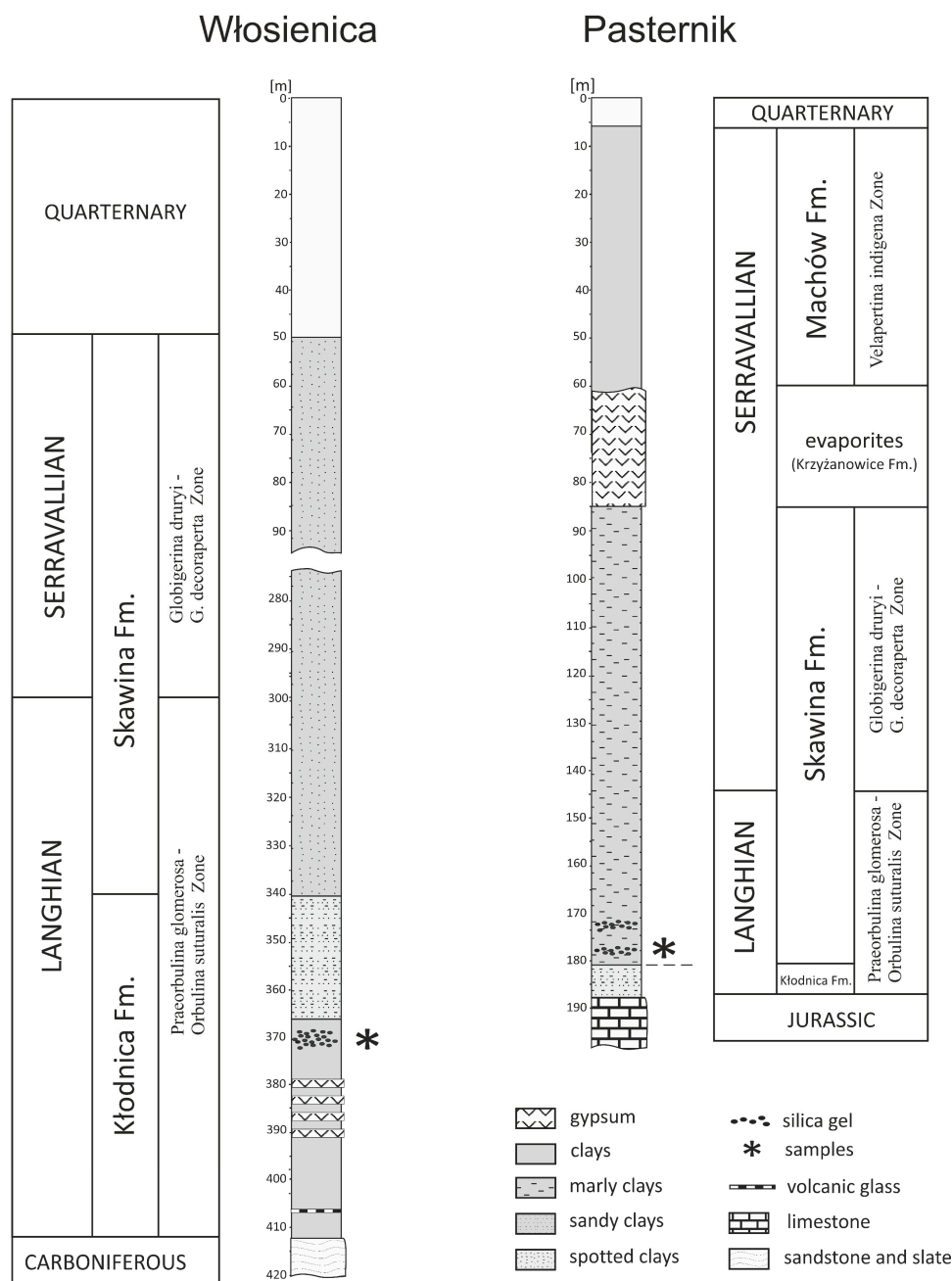


Figure 2. General lithology and stratigraphic position of studied boreholes (after [23]).

3. Materials and Methods

3.1. Materials

The research material containing antimony minerals comes from two borehole sites, known as Pasternik and Włosienica (Figure 1). The Pasternik borehole profile consists of Miocene rocks overlying Upper Jurassic limestones [23]. The lithological profile of the Miocene sediments includes the following: the Kłodnica and Skawina Formations, evaporites (Krzyżanowice Fm) and the Machów Formation (Figure 2). In the Pasternik well, at a depth of 170 to 180 m, within gray and light gray marly clays, a characteristic solidified silica gel containing antimony mineralization was found (Figure 2). The solidified gel occurred in the residuum from slaking clay samples to study microfauna [23]. The gel is represented by crumbled, sharp-edged fragments up to 5 mm in size that may have initially formed one or more layers approximately 0.1–0.2 mm thick. A distinctive feature of each

plate is the presence of oval degassing marks on the upper surface and their absence on the flat, lower surface of the plate (Figure 3A).

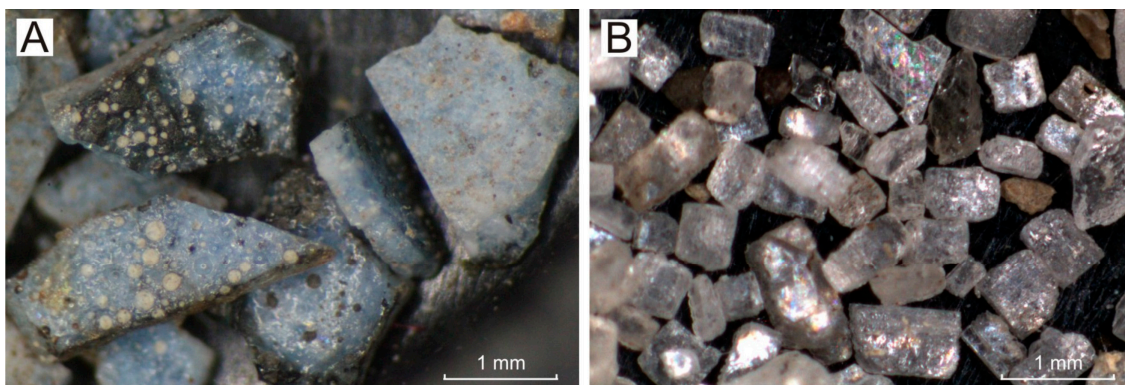


Figure 3. A fragment of solidified light blue silica gel (A) and autogenic crystals of anhydrite (B). Residuum from slaking of sample for the study of microfauna from borehole Włosienica, depth 370 m.

Similar blue solidified silica gel was found in larger amounts in the Włosienica well, located a few kilometers east of Oświęcim (Figure 1). In the drilling profile, Carboniferous sandstones and shales occur in the bedrock (Figure 2). The lithological profile of the Miocene is formed by the Kłodnica and Skawina Formations. Evaporites and younger sediments of the Machów Fm were not observed, probably due to erosion. At a depth of 370 m, a significant accumulation of blue-colored solidified silica gel (with antimony mineralization) was discovered in light green, plastic and layered clays (Figure 2). Within the same residuum sample, a significant accumulation of authigenic, transparent anhydrite crystals, several millimeters in size, were found (Figure 3B).

3.2. Electron Microprobe Analysis (EPMA) and the Backscattered Electron Observations

Backscattered electron (BSE) imaging was obtained using a FEI Quanta 200 FEG scanning electron microscope (FEI Company, Hillsboro, OR, USA), equipped with an EDS detector. The system operated at 25 kV accelerating voltage in high and low vacuum mode.

Electron microprobe studies of brizziite and roméite were performed at the Critical Elements Laboratory AGH-KGHM in Krakow using a JEOL JXA-8230 SuperProbe electron microprobe operating in the wavelength-dispersive mode under the following conditions: accelerating voltage of 15 kV, beam current of 10 nA, beam diameter of 2 μm , peak count time of 20 s, and background time of 10 s. Standards, diffracting crystals, analytical lines and mean detection limits (in wt. %) were as follows: fluorophlogopite–F (PC0, $K\alpha$, 0.12), albite–Na (TAP, $K\alpha$, 0.03), diopside–Mg (TAP, $K\alpha$, 0.02), Si (TAP, $K\alpha$, 0.03), Ca (PET, $K\alpha$, 0.02), orthoclase–Al (TAP, $K\alpha$, 0.03) and K (PET, $K\alpha$, 0.02), stibnite–Sb (PET, $L\alpha$, 0.06), galena–Pb (PET, $M\alpha$, 0.05), bismuthinite–Bi (PET, $M\alpha$, 0.13) rutile–Ti (LPET, $K\alpha$, 0.02), baryte–Ba (PET, $L\alpha$, 0.06), rhodonite–Mn (LIF, $K\alpha$, 0.09), hematite–Fe (LIF, $K\alpha$, 0.08), and sphalerite–Zn (LIF, $K\alpha$, 0.09). The raw data were reduced with the PAP routine of Pouchou and Pichoir. Atomic contents for brizziite were normalized to 3 atoms of oxygen per formula unit (apfu) and for roméite to 2 atoms for the B structural position.

3.3. X-ray Diffraction (XRD) Analysis

Powder X-ray diffraction (XRD) patterns of the solidified silica gel samples rich in intergrowth of brizziite and roméite were recorded at the room temperature with a Rigaku Smart Lab 9.0 kW diffractometer (Rigaku, Tokyo, Japan), under the following conditions: graphite-monochromatized $\text{CuK}\alpha$ radiation with $\lambda = 1.5418 \text{ \AA}$, registration velocity of $0.05^\circ(2\Theta)/1 \text{ s}$, registration range of $2\text{--}70^\circ(2\Theta)$. The data were analyzed using the X'Rayan software (4.2.2) and reference patterns available in the ICDD database.

3.4. Raman Spectroscopy

Raman spectra were collected in the backscattered geometry at the AGH UST, Krakow, Poland, with a Thermo Scientific DXR Raman spectrometer integrated with an Olympus BX 40 confocal microscope and equipped with a 532 nm high power laser (10 mW). The spectra were recorded in the range $3600\text{--}50\text{ cm}^{-1}$ on a randomly oriented surface of crystals mounted in an epoxy resin in a 1-inch disc used for EPMA studies. The Raman measurements were carried out with an estimated analytical spot size of $\sim 1\text{ }\mu\text{m}$, applying the microscope magnification $100\times$, the acquisition time 600 s, and an accumulation of 2 scans.

4. Results

Figure 4A,B present the BSE of the solidified silica gel images, revealing the oval traces of its degassing and dispersed Sb minerals, brizziite and roméite. Apart from the antimony minerals that optically contrast with the silica matrix (BSE images), scatter anhydrite can very rarely be observed.

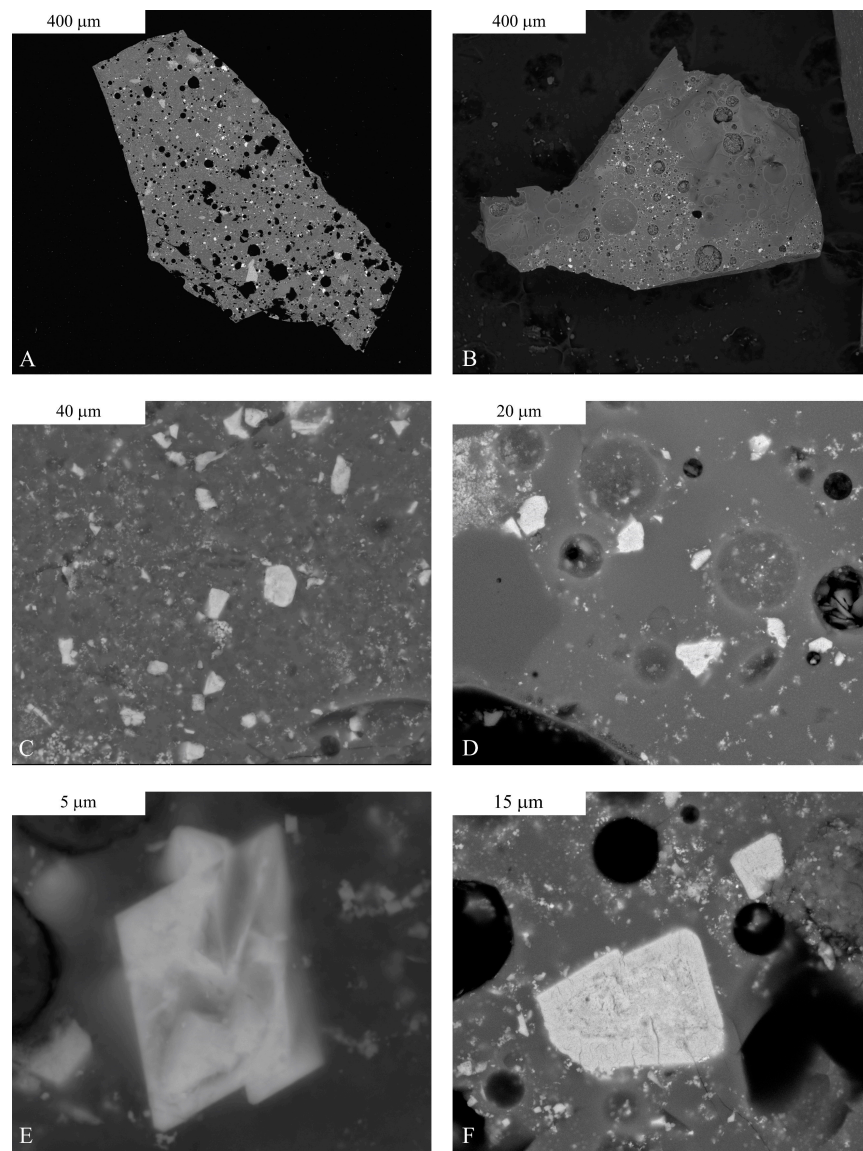


Figure 4. BSE images of the studied Sb minerals scattered in solidified silica; (A–D)–contrasting bright Sb minerals and visible oval traces of degassing; (E)–small idiomorphic crystal of brizziite in solidified matrix; (F)–oval shape of roméite crystal with progressive alterations.

In the solidified silica gel samples, brizziite mainly occurs as a mixture of very small, often poorly formed, grains (Figure 4C,D). The BSE images also show idiomorphic forms or outlines typical of the rhombohedral system (Figure 4E). On some of them, the growth zones can be visible. The roméite is characterized by oval shapes with alterations going inward within the grains (Figure 4F).

The Raman spectrum of brizziite and its comparison with the spectra of the brizziite from two the Italian mines (Cetine (the type locality) and Pereta) [RRUFF database, 2,27] are shown in Figure 5. In the spectrum from the present study, two bands at $\sim 659\text{ cm}^{-1}$ (strong) and 615 cm^{-1} (medium) are similar to the spectra described by Frost [27]; they are attributed to the Sb-O (ν_1) symmetric stretching mode. The weak band at 516 cm^{-1} is ascribed to the Sb-O (ν_3) (antisymmetric stretching vibration). It is shifted by several cm^{-1} towards the lower wave values. Most likely, the band is related to an admixture with roméite, for which the strongest band is 516 cm^{-1} . The presence of minimal substitutions of Ca for Na in the brizziite is also possible. The presence of calcium in the structure of brizziite, with a higher atomic weight than that of Na, shifts the band toward higher wave values. The Raman bands observed at 230, 303, and 312 cm^{-1} are bound to the O-Sb-O bending modes [27].

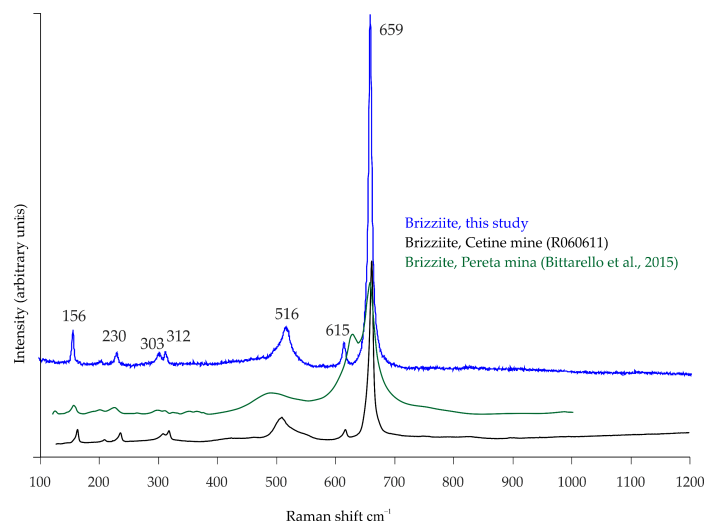


Figure 5. Raman spectra of brizziite with reference data.

The Raman spectrum of roméite (Figure 6) shows the bands which are consistent with the literature data. It should be stressed that roméite is characterized by a wide range of substitutions in the structure, so shifts of some bands are typical of this group of pyrochlores. According to Bahfenne and Frost [28], a strong band at $\sim 517\text{ cm}^{-1}$ for roméite is assigned to the Sb-O (ν_1) symmetric stretching mode, while the medium band at 465 cm^{-1} is assigned to the Sb-O (ν_3) antisymmetric stretching mode. The weak band at ca. 300 cm^{-1} is assigned to the O-Sb-O bending mode. Another medium band has been observed at 828 cm^{-1} . Similar spectral features have also been noted in the roméite samples from Switzerland (791 and 829 cm^{-1}), and Italy (Praborna Mine, 791 and 811 cm^{-1} and Cetine, 791 and 819 cm^{-1}) [28].

The X-ray diffraction patterns of the solidified silica gel have been presented in Figure 7. The main components of the polymineral sample are roméite, brizziite and quartz. The background of the XRD diagram between 15 and 35° 2-theta is slightly elevated, showing that the sample was partially amorphous due to the presence of the silica gel. The best-matched reflections, that are compatible with the reference patterns, belong to quartz and roméite. The shifts in the recorded brizziite reflections may also be related to its substitution of calcium for sodium.

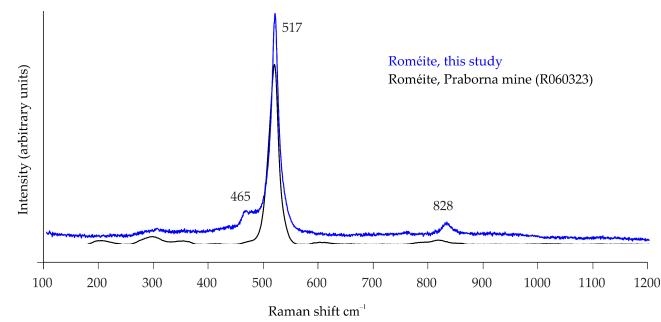


Figure 6. Raman spectra of roméite with reference data.

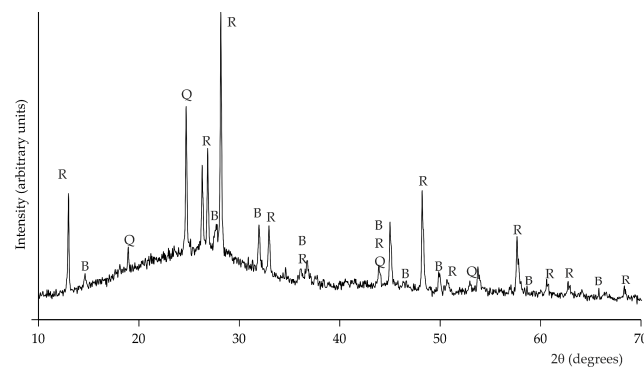


Figure 7. XRD patterns of the solidified silica; visible reflections: brizziite (B), roméite (R) and quartz (Q) (this study).

Tables 1 and 2 show the selected chemical analysis (wt. %) of the grains that correspond to roméite and brizziite. Due to the subtle micro-intergrowths of these minerals, it was impossible to carry out a single analysis from a monomineral part of the brizziite. It has been proven by the admixtures of calcium and fluorine, which most likely come from roméite. As the primary phase, pyrochlore does not form micro-intergrowth with brizziite; however, a part of the pyrochlore grains is altered. Point analyses were carried out on the monomineral grains observed in the BSE images. The formula of roméite has been normalized concerning two cations at the B-site in the structure. The results show that the pyrochlore considered represents fluorcalciroméite. The contents of Ca and Na in the structure are comparable; however, the dominance of one of these cations classifies the mineral to a specific phase. Table 2 shows the exemplary chemical compositions of fluorcalciroméite to the dominant of Na variety.

Table 1. Chemical composition of brizziite from the study localities.

Constituent	wt. %		Constituent	Representative Analysis Normalized on $\Sigma \text{Me} = 2$ (apfu)			
	Min.	Max.		B-1	B-2	B-3	B-4
F	0.00	3.00	F	0.208	0.000	0.148	0.337
Na ₂ O	9.78	11.46	Na ⁺	0.771	0.751	0.715	0.691
SiO ₂	0.35	2.51	Si ⁴⁺	0.000	0.000	0.000	0.000
Al ₂ O ₃	0.07	0.54	Al ³⁺	0.007	0.003	0.004	0.023
MgO	0.00	0.07	Mg ⁺	0.002	0.004	0.003	0.000
MnO	0.00	0.14	Mn ⁺	0.001	0.005	0.002	0.000
BaO	0.00	0.16	Ba ²⁺	0.001	0.000	0.002	0.001
K ₂ O	0.03	0.16	K ⁺	0.003	0.002	0.003	0.007
CaO	2.06	9.37	Ca ²⁺	0.221	0.085	0.145	0.357
TiO ₂	0.00	0.04	Ti ⁴⁺	0.000	0.000	0.001	0.000
PbO	0.05	0.20	Pb ²⁺	0.001	0.002	0.002	0.001
Sb ₂ O ₅	70.40	81.01	Sb ⁵⁺	0.998	1.151	1.127	0.929

Table 2. Representative formulas of roméite from the study localities.

wt. %	R_1	R_2	R_3	R_4	R_5
SiO ₂	3.06	0.27	3.53	1.87	1.42
TiO ₂	0.00	0.00	0.00	0.06	0.00
Al ₂ O ₃	0.17	0.03	0.24	0.05	0.22
Sb ₂ O ₅	70.83	74.38	70.24	75.65	78.10
Bi ₂ O ₃	0.00	0.00	0.00	0.10	0.00
CaO	13.00	14.07	13.01	12.89	12.57
MnO	0.00	0.00	0.00	0.00	0.01
FeO	0.18	0.00	0.04	0.00	0.00
Na ₂ O	6.84	5.97	7.39	7.33	7.09
K ₂ O	0.00	0.02	0.02	0.08	0.11
F	5.09	5.10	5.19	4.89	3.99
H ₂ O _{cal}	0.00	0.00	0.00	0.00	0.00
O = f2	−2.14	−2.15	−2.19	−2.06	−1.68
Total	97.02	97.69	97.48	100.86	101.82
Chemical formula based on Σ B-site = 2 (apfu)					
Na ⁺	0.995	0.837	1.086	1.008	0.940
Ca ²⁺	1.046	1.090	1.056	0.980	0.920
Mn ²⁺	0.000	0.000	0.000	0.000	<0.000
Bi ³⁺	0.000	0.000	0.000	0.002	0.000
K ⁺	0.000	0.002	0.002	0.007	0.009
Σ A site	2.041	1.927	2.142	1.990	1.860
Sb ⁵⁺	1.975	1.997	1.976	1.992	1.982
Ta ⁵⁺	0.000	0.000	0.000	0.000	0.000
Al ³⁺	0.015	0.003	0.022	0.005	0.018
Fe ²⁺	0.010	0.000	0.002	0.000	0.000
Ti ³⁺	0.000	0.000	0.000	0.003	0.000
Σ B site	2.00	2.00	2.00	2.00	2.00
O ^{2−}	5.91	5.92	5.95	5.94	5.95
F	1.209	1.167	1.243	1.097	0.862
A-vac	−0.041	0.073	−0.142	0.010	0.140

5. Discussion

Pasternik and Włosienica are the first localizations of brizziite reported in Poland. The presence of this rare, Sb-bearing mineral in two boreholes, situated several tens of kilometers apart, is worth noting because in each case, the mineralization is hosted within the same rocks of the same geological unit, i.e., the Miocene clays. In the formations dealt with in this study (apart from brizziite) fluorcalciroméite has been recorded.

An additional fact is that an abundant occurrence of antimony minerals in the study area was not found. Only sporadically hydrothermal Sb minerals from the tetrahedrite group were found in the Zn–Pb ore deposit region, 40–50 km north of the study area, [29,30]. The manifestations of the polymetallic mineralization are known from some boreholes and locally on the surface, e.g., in Karniowice and Zalas [31–33]. Both in the Paleozoic basement and in the overlying Mesozoic cover, millerite, bravoite, and cobaltite were noted [34], while other ore minerals included, among others, chalcopyrite, molybdenite, Bi-minerals, scheelite, and traces of Ag, Au, Se, Te, Re, Co and Ni [29,30,35–38]. In recent years, polymetallic mineralization in Zalas has been recognized with such rare minerals as iodargyrite, thought to be indicative of a semi-arid environment in the Miocene, and thalliomelane, a new thallium mineral [32,33]. Mikulski et al. [39] report on trace amounts of antimony from the Zn–Pb ore deposit region, pointing to the importance of Sb as a critical element. Therefore, additional drilling in the studied area of Krakow would help to determine the horizontal extent of antimony mineralization.

Besides the dominant antimony mineralization, single galena grains have been found very rarely. The mineralization occurs in the solidified silica gel, an amorphous substance

containing, in addition to Si, F, Al, Ca, Fe, Na, K, and Mg. It most likely represents a coagulated solution, which is a remnant of the original metal-bearing medium, a warm chloride solution rich in the Sb ions and poor in those of Zn and Pb. The bubbles in the solidified silica gel must have been formed after coagulation of an original gas-rich solution. Their size and distribution suggest a relatively shallow genesis and low pressure. Greater depths and a higher external pressure would not degas.

The solidified silica gel in question is cloudy and blue-colored, probably due to the presence of Sb-bearing compounds. Some literature data report on antimony minerals used as opacifiers and colorings agents in glazed bricks [40] and other ceramics. Calcium and sodium antimonate added to the glaze gave white, yellow, or turquoise color. The present authors observed the blue color in the study samples, but perhaps other chemical admixtures may also result in this color of the silica gel.

Antimony, with an outstanding propensity to migrate, concentrates in low-temperature hydrothermal solutions as an element into post-magmatic residues. The activation and mobilization of antimony are most likely related to the tectonics of the study area during the Miocene rejuvenation of older faults described in this region of the Carpathian Foredeep [41,42]. Warm solutions carrying antimony were transported upwards, with the dislocations closer to the surface. The delivered warmth also influenced the heating of the solutions and the crystallization of the hydrothermal anhydrite observed e.g., in the borehole in Włosienica. During this time (Langhian), sea level changes occurred in the study area [24,42,43], locally creating hypersaline environments where chlorides were delivered to circulating post-magmatic solutions. The slight enrichment of the solutions with Cl^- ions likely effected a further spatial migration of Sb^{5+} . Under appropriate physicochemical conditions, the roméite must have begun its crystallization and solidification of the silica gel.

Foraminifera tests, abundant in the Kłodnica and Skawina Formations, may represent a source of calcium for the pyrochlore. The Ca^{2+} cations in the solutions may also be leached from the underlying Jurassic limestones through which warm antimony-bearing solutions could migrate upwards.

The roméite precipitation proceeded in the solutions with a high calcium activity and a high pH (>7). Thus, its earlier formation at higher Ca concentrations of parental solutions was later limited by local decreases of Ca^{2+} concentrations. This can be seen in the changes in the chemical composition of roméite, revealing a crystallization tendency towards more sodium-bearing phases. Most likely, the composition of the parental solutions changed, and warm solutions caused the changes in the chemistry of pyrochlores, calcium was leached out from the structure and replaced by sodium. The sodium metasomatism took place in an alkaline medium and finally gave rise to brizziite crystallization. The ovalized forms of roméite suggest its dissolution processes from the outer edges. The brizziite could also have precipitated directly from the solution, as evidenced by its idiomorphic crystal forms (Figure 4C). The brizziite crystallization conditions must have also proceeded in solutions with high pH, high salinity, and low concentrations of such metal cations as Zn^{2+} , Pb^{2+} , Mg^{2+} , and Fe^{3+} .

According to one study [44], when the $\text{Na}^+(\text{aq})$ activity is $10^{-0.5}$, the formation of brizziite requires the following activities: of Mg^{2+} below $10^{-2.47}$, Zn^{2+} below $10^{-4.39}$ and Pb^{2+} below $10^{-7.95}$. In contrast, low pH values in the presence of Fe ions would affect the binding of antimony in tripuhyite FeSbO_4 [45].

The literature indicates that, due to the very narrow field of brizziite persistence, its crystallization should be preceded by mopungite [44]. In both earlier type-locations of brizziite in the Italian mines (Cetine and Pereta), mopungite could be the precursor, but due to its very high solubility might have already disappeared, being completely replaced by brizziite.

6. Conclusions

1. Antimony-bearing disseminated mineralization of fluorcalciomroméite and brizziite was found in blue, solidified silica plates in the drill cores of the Miocene marly and layered clays in Pasternik and Włosienica (the Krakow region, Poland). The region is considered the northernmost part of the Central Paratethys.
2. Brizziite was identified previously only in two Italian mines as a secondary Sb mineral formed by deep weathering of primary antimony sulfides. The origin of brizziite in the Miocene sediments may be as a result of (i) alteration of roméite mineralization within supergene zone, or (ii) direct crystallization from Sb^{5+} -rich solutions derived by the leaching of the weathered primary roméite, both processes providing micro- to crypto-intergrowths of these minerals.
3. The repeatability of the Sb-bearing mineralization with brizziite in the Miocene sediments in the Pasternik and Włosienica drill cores is a unique phenomenon because its presence was recorded in the boreholes situated several tens of kilometers apart. The phenomenon may be explained by slight chloride ions delivered to the Miocene groundwater system from drying up seawaters of the Paratethys Sea, mobilizing antimony in the form of chloride complexes, and, eventually, transporting the easily penetrating fluid to the marly and clay Miocene sediments.
4. Antimony is an element that shows the prominent capacity for concentrating and migrating in low-temperature hydrothermal fluids. The absence in the Krakow region of Tertiary (especially Miocene) polymetallic ore mineralization suggests a possible relation of the primary roméite from the rejuvenated Old-Paleozoic polymetallic ore-mineralization present in the basement of the Krakow-Silesia Monocline. Such could result from the uplift and the northward overthrusting of the Carpathian flysch nappes during the Alpine orogeny and the resulting regression of the inland Miocene sea in Central Europe [32].

Author Contributions: B.G., M.P., K.B. wrote the text, prepared most of the figures, and suggested the genetic model of the mineralization; M.P. supplied the samples and developed sediments stratigraphy, B.G. performed micro-Raman spectroscopic, SEM studies and recalculated the EPMA analyses, K.B. performed XRD analyses. All authors have read and agreed to the published version of the manuscript.

Funding: This work was supported by the research grant no 16.16.140.315 from the AGH University of Science and Technology.

Data Availability Statement: Data confirming the results obtained can be obtained upon request from the first author.

Acknowledgments: We thank the anonymous reviewer, and the Editor for their comments that were very helpful in improving the manuscript. We also acknowledge Adam Gawel, Gabriela Kozub-Budzyń, and Adam Włodek for their support during XRD and EPMA data collection, and Adam Pieczka for help with recalculating chemical data, and Andrzej Skowroński for English correction.

Conflicts of Interest: The authors declare no conflict of interest.

References

1. Olmi, F.; Sabelli, C. Brizziite, $NaSbO_3$, a new mineral from the Cetine mine (Tuscany, Italy): Description and crystal structure. *Eur. J. Mineral.* **1994**, *6*, 667–672. [[CrossRef](#)]
2. Bittarello, E.; Cámara, F.; Ciriotti, M.E.; Marengo, A. Ottensite, brizziite and mopungite from Pereta mine (Tuscany, Italy): New occurrences and crystal structure refinement of mopungite. *Mineral. Petrol.* **2015**, *109*, 431–442. [[CrossRef](#)]
3. Sabelli, C.; Vezzalini, G. Cetineite, a new antimony oxide-sulfide mineral from Cetine mine, Tuscany, Italy. *Neues Jahrb. Mineral. Mon.* **1987**, *9*, 419–425.
4. Dessau, G. Antimony deposits of Tuscany. *Econ. Geol.* **1952**, *47*, 397–411. [[CrossRef](#)]
5. Bosi, F.; Christy, A.G.; Hälenius, U. Crystal-chemical aspects of the roméite group, $A_2Sb_2O_6Y$, of the pyrochlore supergroup. *Mineral. Mag.* **2017**, *81*, 1287–1302. [[CrossRef](#)]
6. Atencio, D.; Andrade, M.B.; Christy, A.G.; Gieré, R.; Kartashov, P.M. The pyrochlore supergroup of minerals: Nomenclature. *Can. Mineral.* **2010**, *48*, 673–698. [[CrossRef](#)]

7. Brugger, J.; Gieré, R.; Graeser, S.; Meisser, N. The crystal chemistry of roméite. *Contrib. Mineral. Petrol.* **1997**, *127*, 136–146. [[CrossRef](#)]
8. Ercit, T.S.; Hawthorne, F.C.; Černý, P. Parabariomicrolite, a new species and its structural relationship to the pyrochlore group. *Can. Mineral.* **1986**, *24*, 655–663.
9. Ercit, T.S.; Černý, P.; Hawthorne, F.C. Cesstibtantite—A geologic introduction to the inverse pyrochlores. *Mineral. Petrol.* **1993**, *48*, 235–255. [[CrossRef](#)]
10. Andrade, M.B.; Yang, H.; Atencio, D.; Downs, R.T.; Chukanov, N.V.; Lemée-Cailleau, M.H.; Persiano, A.I.C.; Goeta, A.E.; Ellena, J. Hydroxycalciumicrolite, $\text{Ca}_{1.5}\text{Ta}_2\text{O}_6(\text{OH})$, a new member of the microlite group from Volta Grande pegmatite, Nazareno, Minas Gerais, Brazil. *Mineral. Mag.* **2017**, *81*, 555–564. [[CrossRef](#)]
11. Atencio, D.; Ciriotti, M.E.; Andrade, M.B. Fluorcalcioroméite, $(\text{Ca,Na})_2\text{Sb}^{5+}_2(\text{O,OH})_6\text{F}$, a new roméite-group mineral from Starlera mine, Ferrera, Grischun, Switzerland: Description and crystal structure. *Mineral. Mag.* **2013**, *77*, 467–473. [[CrossRef](#)]
12. Dupont, D.; Arnout, S.; Jones, P.T.; Binnemans, K. Antimony Recovery from End-of-Life Products and Industrial Process Residues: A Critical Review. *J. Sustain. Metall.* **2016**, *2*, 79–103. [[CrossRef](#)]
13. U.S. Geological Survey. *Mineral Commodity Summaries 2020*; U.S. Geological Survey: Reston, VA, USA, 2020; 200p. [[CrossRef](#)]
14. Oszczytko, N.; Krzywiec, P.; Popadyuk, I.; Peryt, T. Carpathian Foredeep Basin (Poland and Ukraine). Its Sedimentary, Structural, and Geodynamic Evolution. In *The Carpathians and Their Foreland. Geology and Hydrocarbon Resources*; Golonka, I., Picha, F.J., Eds.; AAPG Memoir; American Association of Petroleum Geologists: Tulsa, OK, USA, 2006; Volume 84, pp. 261–318.
15. Báldi, K.; Benkovics, L.; Sztanó, O. Badenian (Middle Miocene) basin development in SW Hungary: Subsidence history based on quantitative paleobathymetry of foraminifera. *Int. J. Earth Sci. Geol. Rundsch.* **2002**, *91*, 490–504. [[CrossRef](#)]
16. Kovač, M.; Hudáčková, N.; Halássová, E.; Kováčová, M.; Holcová, K.; Oszczytko-Clowes, M.; Báldi, K.; Less, G.; Nagymarosy, A.; Ruman, A.; et al. The Central Paratethys palaeoceanography: A water circulation model based on microfossil proxies, climate, and changes of depositional environment. *Acta Geol. Slovaca* **2017**, *9*, 75–114.
17. Popov, S.V.; Rögl, F.; Rozanov, A.Y.; Steininger, F.F.; Shcherba, I.G.; Kovac, M. *Lithological-Paleogeographic Maps of Paratethys*; Courier Forschungsinstitut Senckenberg 250; E. Schweizerbart: Stuttgart, Germany, 2004; 46p.
18. Palcu, D.V.; Patina, I.S.; Şandric, I.; Lazarew, S.; Vasiliiev, I.; Stoica, M.; Krijgsman, W. Late Miocene megalake regressions in Eurasia. *Sci. Rep.* **2021**, *11*, 11471. [[CrossRef](#)]
19. Parachoniak, W. Miocene pyroclastic deposits in the foreland of the Polish Carpathians. *Pr. Geol. Kom. Nauk. Geol. PAN Oddz. Krakowie* **1962**, *11*, 5–77. (In Polish)
20. Alexandrowicz, S.W. Lithostratigraphy of the Miocene deposits in the Gliwice area (Upper Silesia, Poland). *Bull. Pol. Acad. Sci. Earth Sci.* **1997**, *45*, 167–179.
21. Bukowski, K.; de Leeuw, A.; Gonera, M.; Kuiper, K.F.; Krzywiec, P.; Peryt, D. Badenian tuffite levels within the Carpathian orogenic front (Gdów-Bochnia area, Southern Poland): Radioisotopic dating and stratigraphic position. *Geol. Q.* **2010**, *54*, 449–464.
22. Bukowski, K.; Sant, K.; Pilarz, M.; Kuiper, K.; Garecka, M. Radioisotopic age and biostratigraphic position of a lower Badenian tuffite from the western Polish Carpathian Foredeep Basin (Cieszyn area). *Geol. Q.* **2018**, *62*, 303–318.
23. Pilarz, M. Micropalaeontological Stratigraphy of the Miocene Deposits in the Kraków-Oświęcim Area. Ph.D. Thesis, AGH University of Science and Technology, Kraków, Poland, 2012; 323p.
24. Ney, R. The role of the “Cracow Bolt” in the geological history of the Carpathian Foredeep and in the distribution of oil and gas deposits. *Prace. Geol. PAN* **1968**, *45*, 1–82. (In Polish)
25. Ryłko, W.; Tomáš, A. Consolidated basement of the Krakow region in the light of the magnetotelluric studies—Main tectonic features. *Biul. Pol. Geol. Inst.* **2010**, *443*, 81–94. (In Polish)
26. Rögl, F. Mediterranean and Paratethys. Facts and hypotheses of an Oligocene to Miocene paleogeography (short overview). *Geol. Carpathica* **1999**, *50*, 339–349.
27. Frost, R.L.; Bahfenne, S. Raman spectroscopic study of the antimonate mineral brizziite NaSbO_3 . *Radiat. Eff. Defects Solids* **2010**, *165*, 206–210. [[CrossRef](#)]
28. Bahfenne, S.; Frost, R.L. Raman spectroscopic study of the antimonate mineral roméite. *Spectrochim. Acta Part A Mol. Biomol. Spectrosc.* **2010**, *75*, 637–639. [[CrossRef](#)]
29. Pieczonka, J. Polymetallic mineralization in Triassic strata of the NW part of the Kraków-Częstochowa Monocline. *Mineralogia* **2010**, *41*, 35–53. [[CrossRef](#)]
30. Karwowski, Ł.; Markowiak, M. Polymetallic mineralization in Ediacaran sediments in the Żarki-Kotowice area, Poland. *Mineralogia* **2012**, *43*, 199–212. [[CrossRef](#)]
31. Czerny, J. Hydrothermal mineralization phenomena in Karniowice Travertine near Cracow. *Mineral. Pol.* **1992**, *23*, 3–13.
32. Gołębiowska, B.; Pieczka, A.; Rzepa, G.; Matyszkiewicz, J.; Krajewski, M. Iodargyrite from Zalas (Cracow area, Poland) as an indicator of Oligocene-Miocene aridity in Central Europe. *Palaeogeogr. Palaeoclimatol. Palaeoecol.* **2010**, *296*, 130–137. [[CrossRef](#)]
33. Gołębiowska, B.; Pieczka, A.; Zubko, M.; Voegelin, A.; Göttlicher, J.; Rzepa, G. Thalliomelane, $\text{TlMn}^{4+}_{7.5}\text{Cu}^{2+}_{0.5}\text{O}_{16}$, a new member of the coronadite group from the preglacial oxidation zone at Zalas, southern Poland. *Am. Mineral.* **2021**, *106*, 2020–2027. [[CrossRef](#)]
34. Muszyński, M. Mineral veins in rocks of the sub-Devonian basement of the Cracow-310 Silesian Monocline. *Zesz. Nauk. AGH* **1991**, *52*, 7–129. (In Polish)
35. Harańczyk, C. Kraków Paleozoic telluric province. *Przegląd Geol.* **1978**, *6*, 337–343. (In Polish)

36. Górecka, E.; Nowakowski, A. Ore deposits associated with acid intrusives and related rocks in the Zawiercie region. *Pr. Inst. Geol.* **1979**, *95*, 97–108.
37. Oszczepalski, S.; Markowiak, M.; Mikulski, S.Z.; Lasoń, K.; Buła, Z.; Habryn, R. Porphyry Mo-Cu-W mineralization within Precambrian-Paleozoic rocks—Prospectivity analysis of the border zone of the Upper Silesia and Małopolska Block. *Biul. Państwowego Inst. Geol.* **2010**, *439*, 339–354. (In Polish)
38. Mikulski, S.Z.; Oszczepalski, S.; Markowiak, M. The occurrence and prospective resources of molybdenum and tungsten ores in Poland. *Biul. Państwowego Inst. Geol.* **2012**, *448*, 297–314. (In Polish)
39. Mikulski, S.; Oszczepalski, S.; Sadłowska, K.; Chmielewski, A.; Małek, R. Trace Element Distributions in the Zn-Pb (Mississippi Valley-Type) and Cu-Ag (Kupferschiefer) Sediment-Hosted Deposits in Poland. *Minerals* **2020**, *10*, 75. [[CrossRef](#)]
40. Holakooei, P.; Ahmadi, M.; Volpe, L.; Vaccaro, C. Early opacifiers in the glaze industry of first millennium BC Persia: Persepolis and Tepe Rabat. *Archaeometry* **2016**, *59*, 239–254. [[CrossRef](#)]
41. Rutkowski, J. Geological Structure of the Cracow Region, South Poland. *Przegląd Geol.* **1989**, *10*, 587–590. (In Polish)
42. Alexandrowicz, S.W. Miocene tectonics in the Upper Silesian Basin. *Acta Geol. Pol.* **1964**, *14*, 175–231. (In Polish)
43. Krach, W. Stratigraphy of the Miocene in the upper Oder and upper Vistula basins, and its correlation with the eastern area of Poland. *Geol. Q.* **1958**, *2*, 82–99. (In Polish)
44. Roper, A.J.; Leverett, P.; Murphy, T.D.; Williams, P.A. The stability of the rare sodium antimonate, brizziite, and its role in Sb mobility. *Mineral. Mag.* **2018**, *82*, 89–93. [[CrossRef](#)]
45. Leverett, P.; Reynolds, J.K.; Roper, A.J.; Williams, P.A. Tripuhyite and schafarzikite: Two of the ultimate sinks for antimony in the natural environment. *Mineral. Mag.* **2012**, *76*, 891–902. [[CrossRef](#)]